Integrated Modeling of the Current Profile in Steady-State and Hybrid ITER Scenarios

W.A. Houlberg[1], C. Gormezano[2], J.F. Artaud[3], E. Barbato[2], V. Basiuk[3], G. Bateman[4], A. Becoulet[3], P. Bonoli[5], L.G. Eriksson[3], A. Fukuyama[6], Yu. Gribov[7], F. Imbeaux[3], J. Kinsey[4], A. Kritz[4], V. Leonov[8], M. Murakami[1], A.Polevoi[7], R. Prater[9], H. St. John[9], ITPA Steady State Operation Topical Group, and ITPA Confinement Database & Modeling Topical Group

[1]ORNL, [2]ENEA Frascati, [3]CEA Cadarache, [4]Lehigh University, [5]PSFC MIT, [6]Kyoto University, [7]ITER IT, Naka, [8]Kurchatov Institute, [9]General Atomics
e-mail contact of main author: houlbergwa@ornl.gov

Abstract. We present integrated modeling of steady-state and hybrid scenarios for ITER parameters, using validated models for the non-inductive current drive sources in conjunction with various theory-based and semi-empirical transport models. A significant benchmarking activity has been undertaken in order to validate the current drive models and reference scenarios. Both cross-code and code-experiment comparisons are reported for NBCD, ECCD and LHCD models. Comparisons are made between simulations and a reference set of experimental discharges selected for their relevance to the ITER steady-state and hybrid scenarios. The aim of the chosen current drive schemes is to optimize the q profile for maximum fusion performance and non-inductive current fraction. Simulations are then performed with various transport modeling codes, self-consistently calculating heating and current drive with ITER design parameters. Operating constraints, such as beta limits and power loss to the divertor, are also taken into account. The simulations address both the final stationary state and dynamic access to it.

1. Introduction

An important goal for ITER has always been to demonstrate reactor scale steady-state operation. This is very challenging, requiring simultaneously operation with a high bootstrap fraction, high beta limits, full non-inductive current drive (NICD) and well aligned plasma current. In addition, all integration aspects have to be demonstrated such as fuelling, impurity accumulation, divertor compatibility, and configuration compatibility with energetic particles confinement. Two scenarios are emerging [1]:

- Steady-state operation in with the objective of 100% non-inductive operation at $Q > 5$. This is referred to as reference scenario-4 ($I_p = 9$ MA). Discharges in existing devices with $q_{95} = 4-5$, $q_{\min} = 1.5-2.5$, $q_0 - q_{\min} < 0.5$ are presently viewed as providing the most promising physics basis for this ITER case.
- A hybrid scenario with the objective of achieving the maximum fluence/pulse. Most promising discharges have flat q profiles with $q_{\min} \approx 1$ and have been demonstrated by the four largest divertor machines to give $\beta_N > 2.5$ under stationary conditions.

A significant benchmarking activity has been undertaken to validate the current drive models and reference scenarios. The status of cross-code and code-experiment comparisons is reported for NBCD, ECCD and LHCD models in Section 2. Integrated modeling of relevant selected experimental discharges and ITER cases is reported in Section 3. A reference set of experimental discharges has been selected on the basis of relevance to the ITER steady-state and hybrid scenarios, and used to validate the modeling codes. The objective of the chosen cases is to optimize the q profile for maximum fusion performance and non-inductive current fraction in ITER. The codes are then used to simulate ITER, self-consistently calculating heating and current drive using design parameters.

2. Current Drive Model Benchmarks

2.1 Negative Ion Neutral Beam Current Drive

In order to penetrate the dense, hot plasmas of ITER, neutral deuterium beam injection energies in the range of 0.5-1.0 1 MeV are required. These energies are much higher than provided by most neutral beam injectors for present day tokamaks, and require the use of negative ion based neutral beams (N-NBI). Two new physics effects are expected to become important in the evaluation of current driven by high velocity beams: multi-step ionization of the fast neutrals in determining the fast ion source profile, and the finite velocity of the fast ions relative to the electrons in determining the plasma shielding response to the fast ion current.

The ionization process was studied in JT-60U by analysis of shine-through measurements for neutral hydrogen energies up to 350 keV/amu [2]. These measurements showed good agreement with calculations that included multi-step ionization processes using the latest reliable atomic data within the experimental error, mainly due to uncertainty in Z_{eff}. Profiles of the non-inductive current density driven by the N-NBI injection at E_B=360 keV have also been measured. Within experimental uncertainty, these results agreed with ACCOME calculations using a multi-step model [3]. ASTRA and ACCOME use similar ionization and Fokker-Planck models and agree well with each other for on and off axis injection [4], but Hobirk, et al. [5] noted that the temporal change in toroidal current in off-axis NBCD experiments in ASDEX Upgrade and JT-60U are smaller than expected from ASTRA simulations. Aside from possible redistribution of fast ions by turbulence or MHD processes, the difference may lie in the model for the neoclassical plasma response to a fast ion current, i.e., the shielding factor, and effects of high plasma toroidal rotation that accompanies all unbalanced NBI experiments. A further complication in analyses is that cases of high NBCD experiments invariably have significant bootstrap current contributions that need to be subtracted from the total current response to evaluate the NBCD component.

The Spitzer response (parallel friction) is easy to calculate and dominates the plasma response at high Z_{eff}, but the trapped particle correction (viscosity) becomes increasingly important at low Z_{eff} and lower aspect ratio (high trapped fraction) and is much more complex. All codes today use simplified forms for the plasma shielding factor that involve various approximations for the trapped particle correction, e.g., large aspect ratio, simplified geometry, zero plasma rotation, and negligible fast ion velocity compared to the electron thermal velocity. Early Fokker-Planck calculations by Start, et al. [6] illustrated the complexity of the problem for low Z_{eff}, finite v_b/v_e, large aspect ratio (=0.03-0.1), and a simplified slowing down distribution. The authors also claimed that the presence of trapped electrons leads to a net current from the thermal ion rotation, which can be viewed as a component of the bootstrap current. These issues have led us to initiate a benchmarking effort to address the adequacy of models for the plasma response in present day and ITER plasmas. A formulation of the friction terms has been generated to arbitrary order in velocity moments, and shows convergence to full Fokker-Planck calculations for both the thermal-thermal and fast-thermal contributions [7]. When these are incorporated in a moments formulation of neoclassical theory [8, 9] and coupled with full Fokker-Planck calculations of the fast ion distributions, they should yield a realistic and computationally efficient (relative to full Fokker-Planck calculations) benchmark against which the various models for the total plasma response can be compared.

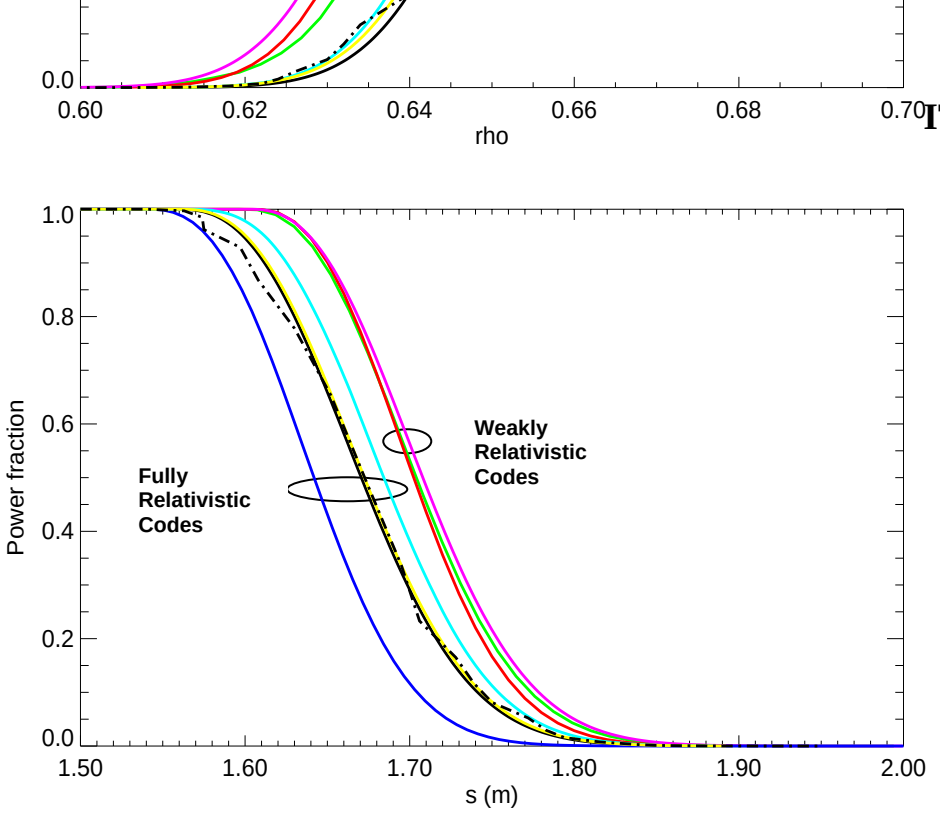

Figure 1: The fully relativistic codes (BANDIT-3D, CQL3D, GENRAY, OGRAY, and TORAY-GA) show slightly stronger absorption than the weakly relativistic codes (ECWGB, TORBEAM, and TORAY-FOM) for the ITER reference case at low density. The position of the 50% absorption fraction has a maximum variation of 7 cm, while the average difference between weakly and strongly relativistic models is ~4 cm.

2.2 Electron Cyclotron Current Drive

A program is underway to validate the computer codes that evaluate the electron cyclotron heating and current drive effects. The Scenario 2 ITER equilibrium and reference kinetic profiles are used, with the EC waves launched near the top of the plasma (R=6.485 m, Z=4.11 m). The participating codes include the Fokker-Planck codes BANDIT-3D [10], CQL3D [11], and OGRAY [12]; the Gaussian beam codes ECWGB [13] and TORBEAM [14]; and the ray tracing codes GENRAY, TORAY-FOM, and TORAY-GA [15]. For the reference conditions the density is low enough that the EC waves travel without significant refraction, so further comparisons are planned at higher density to test the propagation calculations. The wave absorption for the codes is shown in Fig. 1 as a function of arc length along the central ray. The results appear to sort into two slightly different groups, with the fully relativistic codes BANDIT-3D, CQL3D, GENRAY, OGRAY, and TORAY-GA having slightly stronger absorption than the weakly relativistic codes ECWGB, TORBEAM, and TORAY-FOM. This validation process has identified some problems in some codes which have now been rectified. The validation of some of these models against present experiments, combined with results from this code benchmarking activity, provides confidence in the calculations of projections to ITER.

2.3 Lower Hybrid Current Drive

Detailed comparisons between LHCD simulation and experiment are being performed at both the macroscopic and microscopic levels. Several different simulation approaches are being examined for completeness and accuracy, including 1-D and 2-D velocity space Fokker Planck models and adjoint solution methods. A review of benchmarking activities and ITER applications is contained in ref [16]. The predictions of driven LH current for ITER using the most advanced ray tracing-Fokker Planck simulation models available indicate that about 1.6 MA of current will be generated at r/a = 0.6 using 30 MW of injected LH source power.

Furthermore, the local LH current densities should be sufficient to control the point of shear reversal and maintain profiles of negative magnetic shear.

Lower hybrid models typically combine a toroidal ray-tracing module for wave propagation with a numerical solution of the Fokker Planck equation. Ray tracing in tokamak geometry is necessary in order to accurately predict the evolution of the parallel wave number ($k_{//}$), which is important for LH wave accessibility, electron Landau damping, and current drive. Wave propagation models differ little and are based almost exclusively on cold plasma treatment, warm plasma effects being a minor effect on propagation. Treatments of the absorption and calculations of the driven current profile rely upon solutions to the Fokker Planck equation. The sophistication of Fokker Plank models has been varied but has now evolved to full 3-D simulations (r, $v_{\perp}$, $v_{//}$) that self-consistently treat pitch angle scattering, particle trapping, and spatial diffusion in the flux surface geometry. The solution techniques are common to modeling for both LHCD and ECCD and are encapsulated in codes such as BANDIT-3D [10], CQL3D [11], and DELPHINE [17]. With the advent of massively parallel architectures these Fokker Planck simulation codes can now be run routinely within closed loop transport calculations.

The Fokker-Planck and ray tracing models have been quite successful in reproducing the macroscopic features of LHCD experiments such as the experimentally observed current drive figure of merit defined as $\eta_{CD}=<n_e(10^{20}m^{-3})>I\ (A)R_0(m)/P_{LH}(W)$. The LHCD current is typically estimated through a measurement of the loop voltage on the plasma boundary, and then discharges with and without lower hybrid power are compared. An example of such studies were those on PBX-M [18], which demonstrated the dependency of the increased penetration as $n_{//}$ increases. However, as lower hybrid current drive is envisioned as an off-axis current profile control tool in fusion reactor applications, it is important to test our predictive understanding of the physics through measurements of the driven current profile and comparisons with theory. One such approach is to measure the current profile and the loop voltage profile from sequences of equilibrium reconstructions constrained by internal measurements of the magnetic field. For example, profiles of LH current density have been inferred in an LHCD dominant JT60-U plasma [19]: the total current was determined from MSE measurements, while the bootstrap and NB currents were computed numerically; the DC electric field that drives the Ohmic current was evaluated from temporal evolution of the poloidal flux that was obtained from MSE analysis; and the LH current density was deduced from $J_{LH}=J_{TOT}-J_{BS}-J_{NBI}-J_{OH}$. The comparison between the evaluated LH current profile and the combined ray tracing – Fokker Planck calculation in the ACCOME code [20] showed very good agreement.

LHCD simulation models have also been benchmarked against experiment at a more microscopic level. Fast electrons generated in LHCD experiments are characterized by energies that are typically in the range of 100 – 300 keV. One important point of disagreement between simulation and experiment has been attributed to fast electron diffusion effects in the computation of the rf power deposition and current density profiles. It is expected that fast electron diffusion will become less of a concern as one proceeds to the reactor regime for several reasons. First, when moving to high-density fast electrons tend to thermalize before they diffuse. This tendency has been shown clearly in an LHCD experiment on FTU [21], as illustrated in Fig. 2. The HXR emissivity profile was broader than the modeled current density profile at low density, while at high density the two profiles agreed fairly well, indicating that the slowing down process of fast electrons took place on a time scale faster than the radial diffusion time. Second, reduced wave accessibility at higher

density requires lower phase velocity waves resulting in lower energy electrons, which in turn take less time to thermalize. Finally, the fast electron confinement time τ_F should be longer in a larger device since the bulk energy confinement time is longer.

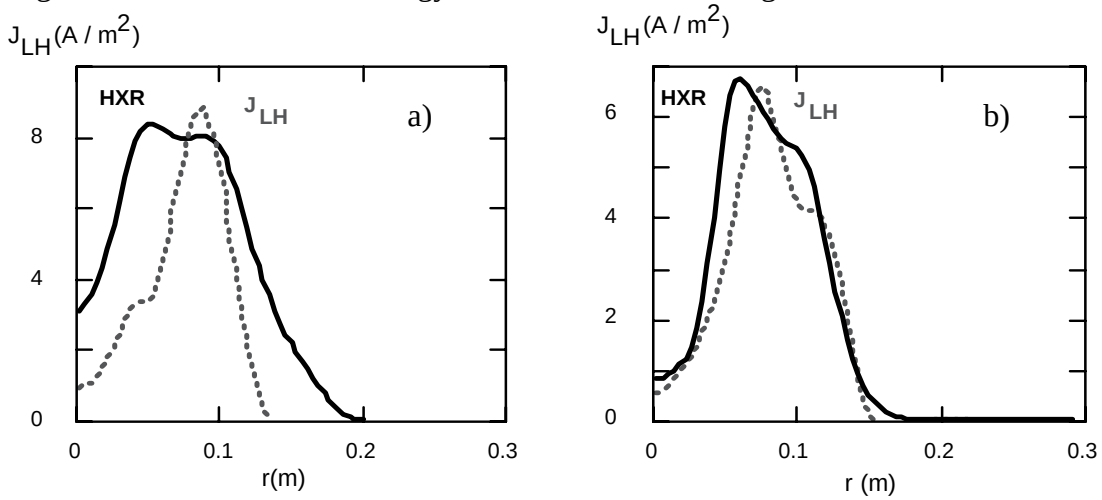

Figure 2: HXR profile in FTU a) is broader than the calculated LH current profile, indicating possible diffusion of fast electrons that are not in the computed profile, while b) at higher density the agreement indicates that spatial diffusion is reduced. From ref [20].

3. Integrated Modeling of the Current Profile

Complex interactions amongst transport, bootstrap current, non-inductive current drive sources, equilibrium, etc., require a high level of physics model integration with consistent treatment of temporal and spatial effects. Several predictive time-dependent modeling codes that integrate these models are being validated against reference experimental cases and contributing to the effort to provide a more complete analysis of ITER steady-state and hybrid operation scenarios.

3.1 Benchmarking Against Existing Experiments

CRONOS [22] operates on the Tore Supra, JET, FTU and ITPA databases, and incorporates the GLF23 [23] and Weiland transport models. The focus of its ITER relevant applications is the interpretative simulation of JET steady-state advanced operation mode, which relies on a plasma current profile pre-shaping phase that optimizes plasma current ramp-up and LHCD to reach the target steady-state q-profile as soon as possible in the discharge.

The ONETWO code uses the retuned GL23 model [23] in validation against recent DIII-D experiments that aim at fully non-inductive operation at high beta. Comparison between calculations and experimental evolution toward the stationary state of a discharge with a 90% non-inductive fraction is reported in [24]. The T_e, T_i and toroidal momentum equations are solved with self-consistent source and sink calculations by time stepping from initial profiles over several confinement times. The density profile is fixed using the experimentally measured profile at one time. The other calculated profiles are in good agreement with experimental profiles. Steady-state performance with the Ohmic current completely relaxed is calculated by a globally convergent modified Newton method.

Corsica [25] has been used to model a variety of DIII-D discharges including ELMing H-mode, strong negative central shear (NCS), quiescent double barrier (QDB) and QH-modes.

Extrapolation to steady-state using current profile control to maintain internal transport barriers was explored for the NCS and QDB conditions. The NCS simulations included feedback modelling of the EC antenna aiming to control the q profile with ECCD [26].

TASK is a new code being developed in Japan. Systematic comparison with experimental data on JT-60 and the ITPA database is under way.

3.2 Simulation of ITER Steady-State and Hybrid Scenarios

The ONETWO code with the GLF23 transport model is being applied to simulation of the ITER steady-state reference scenario-4 using: (1) two negative ion based neutral beam injectors (33 MW at 1 MeV D) tiled vertically, (2) fast wave CD (20 MW at 56 MHz), whose fraction is adjusted using co- and counter-phasing with variable dwell times, and (3) midplane-launched EC power of 20 MW at 170 GHz, providing off-axis current at r/a = 0.4. While plasma density profiles are prescribed, the electron and ion temperature and toroidal rotation velocity profiles are evolved with boundary conditions imposed at ρ=0.9. The helium ash density is set using n_{He}/n_e=4 %, and with the prescribed carbon profile yields Z_{eff} = 1.2 in the core region ($\rho \leq 0.4$) and Z_{eff}= 2 near the plasma edge. The MHD equilibrium is taken from a DIII-D like AT equilibrium used in a previous studies [27]. Since the core temperature depends strongly on the edge temperature due to the stiff transport model, scans of an assumed edge temperature value are used to generate the Q~5 case of Fig. 3. There are some differences depending on whether the NCLASS [9] or Sauter [28] models are used for the bootstrap current. More details of these scans are given in [24]. These parameters correspond to the 0-D operation space of fusion performance figure of merit, $\beta_N H_{89}/q_{95}^2 = 0.27$ with $f_{BS} > 50$. Important physics issues that are yet to be addressed include: consistency of the pedestal conditions, divertor heat load, and stability (in particular RWM and error field effects).

The CRONOS suite is being used to investigate the complete time sequence from X-point formation to steady-state, and the relative role played by the various heating and CD sources, including bootstrap current, and off-axis LHCD or ECCD. The simulations focus on the pre-shaping capability of the ITER current profile, the possibility of fully non-inductive operation, and the feasibility of steady-state operation. Similar to observations in JET, ITER transits easily into an ITB regime during the current ramp-up phase, provided that the current ramp rate is on its high-value side (~0.15-0.2 MA/s). The superposition of central ICRH (2^{nd} harmonic T), and/or N-NBI helps slow the Ohmic current penetration and maintains a reversed shear situation at least through the current ramp phase. The addition of off-axis CD (provided, for example, by 20 MW of LHCD that peaks at mid-radius) is a powerful supplementary asset in this pre-shaping phase, which helps in driving the discharge along a stable MHD path (although real time feedback loops are yet to be developed). The typical behavior of the ITER simulations is a transition from an L to an H+ITB mode at about 5-6 MA when heat transport allows conditions sufficient to insure the produce 40-80 MW of alpha power, i.e. to reach Q~5. A fully non-inductive situation consists of ~60% bootstrap, ~20% LHCD, and ~20% NBCD, consistent with 0-D predictions. But with or without off-axis LHCD, such a target is found to be non-stationary. The bootstrap current profile is dominated by the edge pedestal contribution and by a large peak at the ITB around mid-radius (driven by the temperature gradient). This peak tends to lie slightly inside the ITB region and slowly shrinks both the ITB and the minimum shear regions. The severe misalignment of the pressure and current profiles brings the discharge back to stationary, but much lower Q~ 2, and f_{NI}~ 60-70% after 1 to 2 current diffusion times (i.e. 200-400 s). To counteract this ITB shrinking, an off-axis current peak in the positive magnetic shear region must be driven with

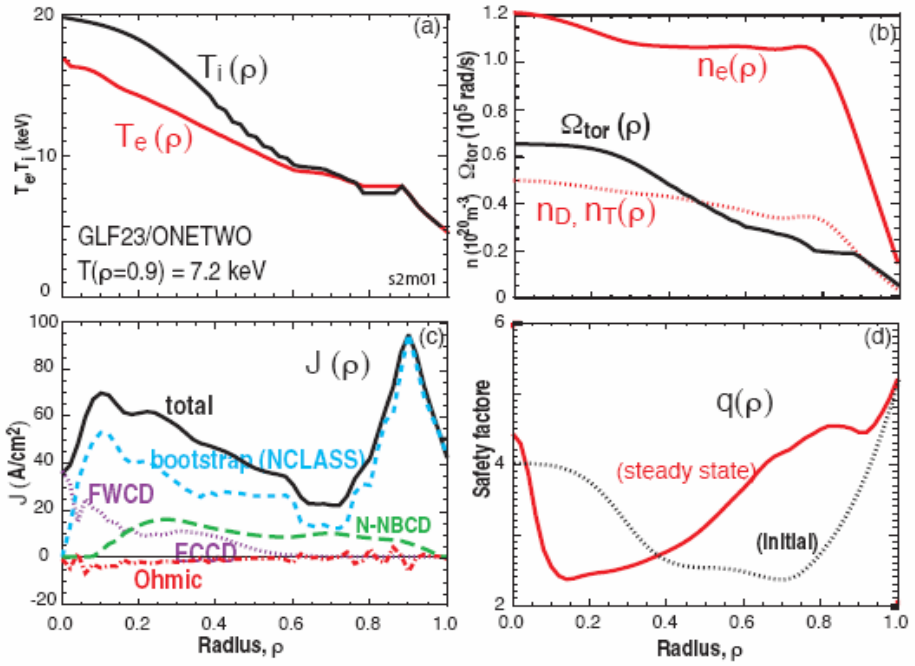

Figure 3: The profiles for ITER steady-state scenario 4 [1] from the ONETWO code with the GLF23 transport model: a) temperatures, b) densities and toroidal rotation, c) current contributions, and d) the initial and final q profiles.

current density sufficient to balance the bootstrap effect. From these preliminary results we conclude that: 1) a very high bootstrap current fraction (80-90%) with ITBs combined with a flat density profile may need a localized current source near the ITB, and 2) with the present input powers, off-axis CD schemes that provide the greatest localization and efficiency are favored. More work is underway to optimize the scenarios and improve the physics elements.

ASTRA has been used to simulate the whole dynamics of ITER operational scenarios [29]. Although for the steady-state scenarios the core transport model is simplified, other more comprehensive physics components include: 1) boundary conditions from B2-Eirene, 2) evolution of the density profile, and 3) evaluation of MHD effects [30]. $H_{98(y,2)}$ =1.3-1.5 is required to reach steady-state operation, but is above the ideal MHD no wall limit and requires active RWM control. The stable operating space shrinks with pressure peaking. If $H_{98(y,2)}$ can be increased to 1.5-1.7 the required non-inductive current can be achieved with 33 MW NBCD and 20 MW ECCD with operation below the ideal limit[31].

ITER cases being simulated by Corsica include steady-state discharges with ITBs. In these simulations, the barrier is formed by reducing transport coefficients at a radial location typically chosen to be near q_{min}. New capabilities for operation with a plasma control system are currently under development. This will provide the capability for studying a variety of feedback control issues needed to sustain for steady-state and hybrid scenarios in ITER.

4. Summary

It is important to note that because the attainable Q is inversely proportional to the auxiliary power, we must maximize reliance on the bootstrap current supplemented by the most efficient application of auxiliary CD sources. This has driven us to develop a comprehensive plan within the ITPA to benchmark the heating and CD models under expected ITER steady-state and hybrid conditions. Good progress is being made in these benchmarks, but several issues remain. Our general conclusions are the reversed shear profiles are achievable only if

full heating and CD capabilities are present and by operating at high T_e. An effective CD technique on the outer part of the plasma is needed for control of the profile. This is provided either by using LHCD or by allowing the pedestal to reach quite high temperature values, which yields a high bootstrap current at the edge. But because of the complexity of the interactions between current evolution, MHD stability, transport, and boundary effects, there is still a lot of work ahead before the simulations contain sufficiently comprehensive physics to define optimal scenarios and control requirements. Additional modeling efforts not covered here broaden the analysis of ITER scenarios, e.g.: TASK simulations of ITER steady-state simulations; BALDUR and JETTO efforts to integrate models for the pedestal and ELM dynamics with the core physics; and TRANSP analysis that has focused on testing transport models against a selection of high performance discharges in the ITPA Profile Database to see how well they compare with the best confinement conditions attained in present devices.

References

[1] SHIMOMURA, Y., et al., Plasma Phys. Control. Fusion **43** (2001) A385.
[2] SUZUKI, S., et al., Plasma Phys. Control. Fusion **40** (1998) 2097.
[3] OIKAWA, T., et al., Nucl. Fusion **41** (2001) 1575.
[4] POLEVOI, A., SHIRAI, H., TAKIZUKA, T., JAERI Report 97-014 (1997).
[5] HOBIRK, J., et al., 2003 Proc 30th EPS Conf. on Control. Fusion and Plasma Phys. (St. Petersburg) ECA **vol 27A**, O-4.1B.
[6] START, D.F.H., CORDEY, J.G., JONES, E.M., Plasma Phys. **22** (1980) 303.
[7] HIRSHMAN, S.P., private communication, Sept 2004, to be presented at the 2004 DPP-APS meeting.
[8] HIRSHMAN, S.P., SIGMAR, D.J., Nucl. Fusion **21** (1981) 1079.
[9] HOULBERG, W.A., et al., Phys. Plasmas **4** (1997) 3230.
[10] O'BRIAN, M.R., et al., Proc. IAEA TCM on Advances in Simulation and modeling of Thermonuclear Plasmas, Montreal, Canada, 1992 (IAEA, Vienna, 1993) 527.
[11] HARVEY, R.W., McCOY, M.G., Proc. IAEA TCM on Advances in Simulation and modeling of Thermonuclear Plasmas, Montreal, Canada, 1992 (IAEA, Vienna, 1993) 498.
[12] ZVONKOV, A.V., et al., Plasma Phys. Reports **24** (1998) 389.
[13] CIRANT, S., NOWAK, S., OREFICE, A., J. lasma Phys. **53** (1995) 345; NOWAK, S., LAZARRO, E., RAMPONI, G., Phys. Plasmas **3** (1996) 4140.
[14] POLI, E., PEREVERZEV, G.V., PEETERS, A.G., Phys. Plasmas **6** (1999) 5; POLI, E., et al., Fusion Eng. Design **53** (1999) 9.
[15] KRITZ, .H., et al., Proc. 3rd Int. Synp. On Heating in Toroidal Plasmas, Grenoble, Italy, 1982, Vol. II (ECE, Brussels, 1982) 707; MATSUDA, K., IEEE Trans. Plasma Sci. **17** (1989) 6.
[16] BONOLI, P.T., et al., 2003 Radiofrequency Power in Plasmas, AIP Conf. Proc. vol 694, ed C.B. Forest, p.24.
[17] SHOUCRI, M. SHKAROFSKY, I., Comput. Phys. Commun. **82** (1994) 287.
[18] BERNABEI, S., et al., Phys. Plasmas **4** (1997) 125.
[19] NAITO, O., et al., Phys. Rev. Lett. **89** (2002) 065001.
[20] DEVOTO, R.S., et al., Nucl. Fusion **32** (1992) 773.
[21] BARBATO, E., et al., Fusion Sci & Technol. **45** (2004) 323.
[22] BASIUK, V., et al., Nucl. Fusion **43** (2003) 822.
[23] KINSEY, J.E., et al., Proc. 19th Int. Conf. on Fusion Energy (Lyon, 2002) (Vienna: IAEA) TH/P1-09.
[24] MURAKAMI, M., et al., this conference, IAEA-CN-116/EX/1-2.
[25] CROTINGER, J.A., et al., LLNL Report UCRL-ID-126284, 1997.
[26] CASPER, T.A., et al., Plasma Phys. Control. Fusion **45** (2003) 1.
[27] LAO, L.L., et al., Nucl. Fusion **43** (2003) 1043.
[28] SAUTER, O., et al., Phys. Plasmas **4** (199) 2834.
[29] ITER Technical Basis, ITER EDA Documents Series No. 24, IAEA, Vienna, 2002.
[30] POLEVOI, A., et al., Proc. 19th Int. Conf. on Fusion Energy (Lyon, 2002) (Vienna: IAEA) CT/P-08.
[31] POLEVOI, A.R., et al., this conference, IAEA-CN-116/IT/P3-28.